A Model for the Inertial Capture of Particulates in a Bubbling Filter

N.P. Kristensen and R.D. Braddock

Griffith University, Nathan, Queensland, 4111, Australia (r.braddock@mailbox.gu.edu.au)

Abstract: The bubbling filter has efficiencies comparable to the wet scrubber at a reduced pressure drop. However, the mechanisms by which the filter functions are not entirely understood. Experimental studies show the formation of tortuous pathways within the filter and suggest that inertial capture of particulates may be a key mechanism. This paper uses an ideal flow approximation to model the flow along the tortuous pathway through the filter. Linear and nonlinear drag laws are used to calculate the trajectories of particles in the airflow, and to assess their capture on the sides of the flow path. The calculated efficiencies are compared with the experimental estimates of the removal efficiency. Some comments are also made on the removal processes operating in the bubbling filter.

Keywords: Bubbling filter; Inertial capture; Mathematical model

1. INTRODUCTION

The bubbling filter consists of a fibrous filter irrigated with water as shown in Figure 1.

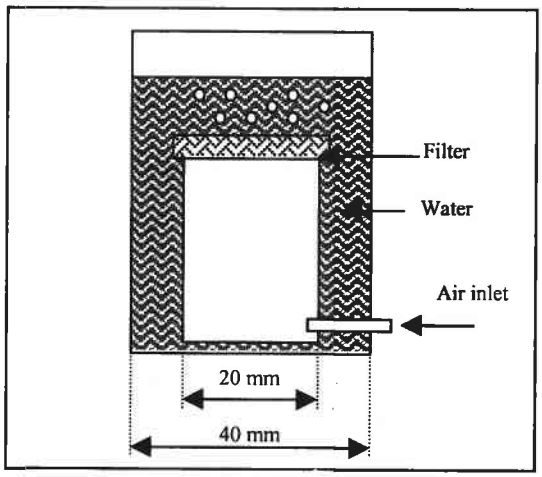

Figure 1: The bubbling filter (adapted from Agranovski et al., 1999a).

The bubbling filter has efficiencies comparable to the wet scrubber for particles in the 1 – 10 μm particle diameter range. In contrast to the wet scrubber, the pressure drop (and hence the energy and cost required) is lower. It was demonstrated that the capture of particulates within the bubbling filter could be described using the bubble theory of Fuchs [Agranovski et al., 1999a].

Fuchs [1964] describes the formation of vortices within a rising bubble leading to particle capture as described by Equation (1):

$$\frac{dC}{dx} = -(\alpha_i + \alpha_s + \alpha_d)C, \qquad (1)$$

where α_i is the inertial capture coefficient, α_s is the sedimentation capture coefficient, α_d is the molecular diffusion coefficient, and C(x) is the concentration of particulates as a function of the vertical rise distance, x. Agranovski et al. [1999b], however, demonstrated that increasing the depth of water above the fibrous section of the filter (which increases rise distance x) did not increase capture.

A Nuclear Magnetic Resonance (NMR) image of a vertical slice through the filter was taken [Agranovski et al., 1999b]. It was found that a tortuous preferential pathway of air developed within the filter, and it was proposed that inertial capture of particles as they negotiate this pathway was the primary mechanism behind particle collection [Agranovski et al., 1999b].

Agranovski et al. [2000a] proposed a model for the air flow through the pathway. Given that the flow within the pathway is laminar [Agranovski et al., 2000a; Agranovski et al., 2000b] and the

assumptions that the fluid flow is ideal, i.e. steady state, incompressible, inviscid and irrotational, the fluid flow may be described as:

$$u = -\nabla\phi, \tag{2}$$

where ϕ is the potential function and u is the velocity vector [Evett and Lin, 1987]. Substituting in the continuity equation then yields Laplace's equation:

$$\nabla^2\phi = 0. \tag{3}$$

Agranovski et al. [2000a] solved Equation (3) in the major air pathway through the NMR image from Agranovski et al. [1999b] using the PDE Toolbox in MATLAB™. This solution provided the streamlines of the flow of the carrier gas through the filter. This paper aims to model the inertial capture of the particles by the filter.

2. METHOD

2.1 Overview

The flow field information by Agranovski et al. [2000a] was exported to the Graphical User Interface (GUI). The velocity field, geometry and mesh information were saved and input into a program designed to calculate the trajectory of particles through the geometry in two dimensions. The program is based on Newton's Second Law, relating the momentum change of each particle to the forces acting upon it.

2.2 Forces Acting Upon the Particle

The forces assumed to act upon the particle were drag, gravity and buoyancy. The force of drag, F_D, on a spherical particle of radius r_p is described in Cartesian coordinates [Hinds, 1982]:

$$F_D = C_D\left(\frac{\pi}{8}\right)d_p^2\rho_p\left[\left(x_f' - x_p'\right)^2 + \left(y_f' - y_p'\right)^2\right]^{1/2} \left[\left(x_f' - x_p'\right)\underline{i} + \left(y_f' - y_p'\right)\underline{j}\right] \tag{4}$$

where C_D is the coefficient of drag, d_p is the particle diameter and ρ_p is the particle density. (x_p, y_p) is the vector position of the particle in cartesian coordinates, hence x_p and y_p are the particle velocity components, and $\underline{i}$ and $\underline{j}$ are oriented in the 'positive' directions (up and to the right respectively). x_f and y_f are the fluid x and y velocity components respectively (exported from the PDE Toolbox).

The coefficient of drag, C_D, was varied depending upon Reynold's Number, **R** [Hinds, 1982; Prandtl and Tietjens, 1934]. For the Stoke's region ($0.001 \le \mathbf{R} < 1$):

$$C_D = \frac{24}{\mathbf{R}C_c}, \tag{5}$$

where C_c is the slip correction factor (Hinds, 1982). For the transition region ($1 \le \mathbf{R} < 5$):

$$C_D = \frac{24\left(1 + 0.0916\mathbf{R}\right)}{\mathbf{R}C_c}. \tag{6}$$

For the transition region ($5 \le \mathbf{R} < 1000$):

$$C_D = \frac{24\left(1 + 0.158\mathbf{R}^{(2/3)}\right)}{\mathbf{R}C_c}. \tag{7}$$

For a region subject to pressure drag ($1000 \le \mathbf{R}$):

$$C_D = 0.4. \tag{8}$$

Gravity, F_G, and buoyancy, F_B, were described by:

$$F_G = -9.81(4/3)\pi r_p^3\rho_p\underline{i}, \tag{9}$$

$$F_B = 9.81(4/3)\pi r_p^3\rho_d\underline{i}. \tag{10}$$

2.3 Describing Particle Capture

Combining equations (4) - (10) into Newton's Second Law gives:

$$m_p\left(x_p''\underline{i} + y_p''\underline{j}\right) = \Sigma F, \tag{11}$$

where m_p is the mass of the particle. Equation (11) was rewritten as a system of four ordinary differential equations. Letting

$$J' = \begin{bmatrix} j_1' \\ j_2' \\ j_3' \\ j_4' \end{bmatrix} = \begin{bmatrix} x_p' \\ x_p'' \\ y_p' \\ y_p'' \end{bmatrix}, \tag{12}$$

then a vector system of four ordinary differential equations is given by Equation (13):

$$J' = \begin{bmatrix} j_2 \\ \left(\frac{1}{m_p}\right) C_D \left(\frac{\pi}{8}\right) d_p \rho_p \left[(x'_f - j_2)^2 + (y'_f - j_4)^2\right]^{1/2} (x'_f - j_2) \\ j_4 \\ g + \left(\frac{1}{m_p}\right)\left(g\left(\frac{4}{3}\right)\pi r_p^3 \rho_f + C_D \left(\frac{\pi}{8}\right) d_p \rho_p \left[(x'_f - j_2)^2 + (y'_f - j_4)^2\right]^{1/2} (y'_f - j_2)\right) \end{bmatrix}. \quad (13)$$

Initial conditions were given by:

$$(x_p, y_p)(t=0) = (x_o, y_o), \quad (14)$$

$$(x'_p, y'_p)(t=0) = (x'_f, y'_f). \quad (15)$$

To save computational time the particle initial positions, (x_o, y_o), were placed just below where the streamlines were observed to start curving significantly. The cylinder containing the filter was lengthened to prevent the upper and lower boundaries of the cylinder from affecting the shape of the streamlines as described by Agranovski et al. [2000a]. Also, in Equation (15) the particle velocity is assumed to initially be in equilibrium, that is, travelling with the air flow. These initial conditions and the assumptions made in determining them are justified by calculating the relaxation time for the particles (a measure of the time taken for a particle in a uniform flow field to reach equilibrium), estimated to be 10^{-6} – 10^{-8} seconds [Hinds, 1982].

The program used the MATLAB™ ODE45 solver to solve Equation (13) for (x_p, y_p) the position of the particle, at each time step. This gave the trajectory of the particles.

Particles were run through the filter individually, thereby ignoring interaction between particles including agglomeration and particle bounce. It was assumed that when a particle trajectory crossed the geometric boundary they were captured on the air-water interface and absorbed into the filter so no re-entrainment occurred.

For the purpose of producing results to compare with empirical results, the parameter values used by Agranovski et al. [1999a] were used in the program:

- Particle diameter of 2.7 μm (r_p = 1.35 μm);
- Filter face velocities of 0.5 m/s ($x'_f = 0.5 m/s$, $y'_f = 0 m/s$); and
- Particle density, ρ_p, of 914 kg/m^3, being the density of Di-ethyl-hexyl-sebecate used in experiments.

3. RESULTS

3.1 NMR Image Geometry

The results are shown in Figure 2, which is a reproduction of the NMR image in Agranovski et al. [1999b] within the MATLAB™ PDE Toolbox. The major air pathway can be seen running through the filter on the middle left and the fingers formed within the filter are included.

Particle trajectories are shown by lines starting at the bottom of Figure 2 and moving up through the pathway. Figure 2 shows that particles are not captured and, when compared to the results of Agranovski et al. [2000a], do not significantly deviate from the streamlines.

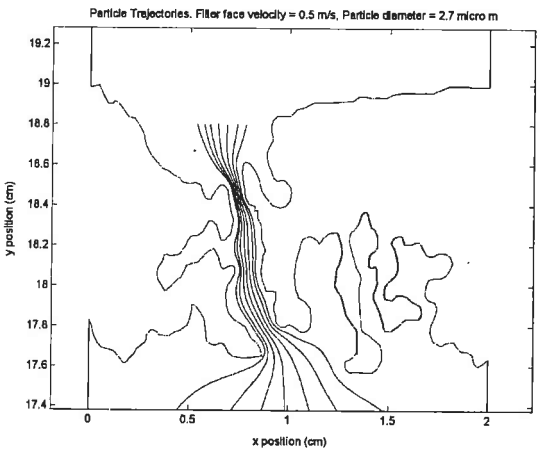

Figure 2: Seven particle trajectories through the NMR image of the filter for a particle diameter of 2.7 μm and a filter face velocity of 0.5 m/s.

Increasing the face velocity to 10 m/s gives the particle trajectories shown in Figure 3, which shows the particle trajectories through the pathway.

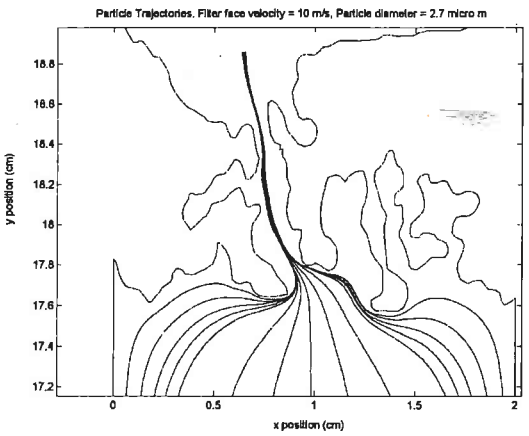

Figure 3: Fifteen particle trajectories through the NMR image of the filter for a particle diameter of 2.7 μm and a filter face velocity of 10 m/s.

From Figure 3 it can be seen that particles will tend to deviate from the streamlines more due to their increased inertia. This is apparent from particle trajectories crossing one another, which streamlines cannot do. The crossing of particle trajectories brings into question the validity of the assumption that particle trajectories may be considered independently of one another. Details on inter-particle interactions such as the possibility of particle collision, bounce and agglomeration (which will effect particle diameter and hence inertial capture) are yet to be investigated.

The reasons behind the lack of inertial particle capture could be a combination of the compensatory effects of streamline curvature, velocity and the tortuousity of the pathway.

The streamline separation and streamline velocity bear an inverse relationship to one another. Inertial effects on the particles will depend on curvature as well as separation of the streamlines The inertial capture of particles is greatest when the streamlines are most curved and when the velocity is great. However, in the NMR image, the greatest curvature of streamlines occurs just below the filter where the velocity is relatively low but increasing. Conversely, the highest velocity will be found where the cross-sectional area is lowest, that is within the pathway through the filter. However, the pathway and its section of the streamlines are relatively straight.

The importance of having a tortuous pathway through the filter is to simultaneously increase streamline velocity and streamline curvature. Interestingly, it is also expected that pathway tortuousity and velocity will also bear an inverse relationship, i.e., that increasing the face velocity through the filter will tend to straighten out the pathways formed by increasing the pressure on the air-water interface. The extent to which this applies will require further investigations in NMR imaging.

3.2 Increasing the Tortuousity of the Pathway

To investigate the effects of tortuousity of the filter pathway, an arbitrary geometry was formed in the PDE Toolbox using the same methods described by Agranovski et al. [2000a] as shown in Figure 4.

The arbitrary geometry was designed to have similar attributes (length, width and general shape) to the NMR image except that the pathway is more tortuous. The tortuousity [Bear, 1972] of the major pathway in the arbitrary geometry is 1.6 as opposed to 1.2 for the original NMR image.

Particle trajectories for a filter face velocity of 0.5 m/s and a particle diameter of 2.7 μm were generated as shown in Figure 4. As can be seen from Figure 4 particles are captured within the arbitrary geometry. The particles captured had initial x_0 positions of 0.1 and 0.15 cm from the left edge, and are captured on the lower boundary of the filter when they fail to negotiate the bend into the pathway. Those particles that are nearer to the center of the filter are not captured within the pathway.

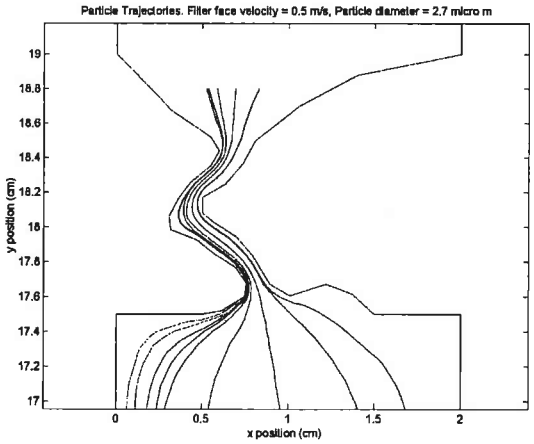

Figure 4: Nine particle trajectories through the arbitrary geometry for a particle diameter of 2.7 μm and a filter face velocity of 0.5 m/s.

Increasing the face velocity to 5 m/s gives the particle trajectories shown in Figure 5. All particles are captured. Some are captured near the

bottom of the filter similar to those seen in Figure 4, and the rest are captured within the pathway. Figure 5 was generated using a coarser mesh than Figure 4 for expedience. The meshes may be viewed in Figure 7 and Figure 7.

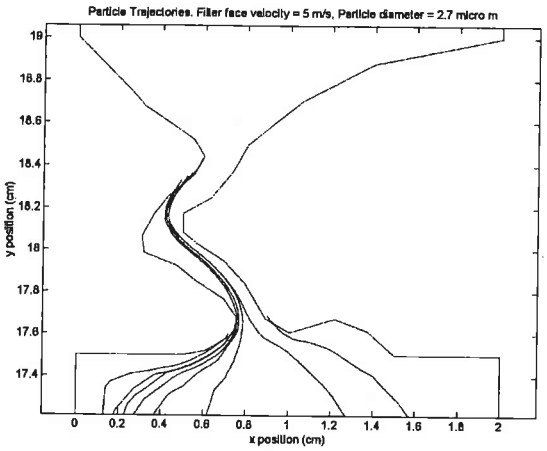

Figure 5: Eight particle trajectories through the arbitrary geometry for a particle diameter of 2.7 μm and a filter face velocity of 5 m/s.

When Figure 5 is compared with Figure 3 (which used a greater filter face velocity, 10 m/s), the effect of increasing the tortuousity of the pathway becomes apparent. It can also be seen from Figure 5 that some of the particle trajectories exhibit discontinuities. This is due to the coarser mesh used in the PDE Toolbox. The discontinuities appear where the particle moves from one mesh element to another.

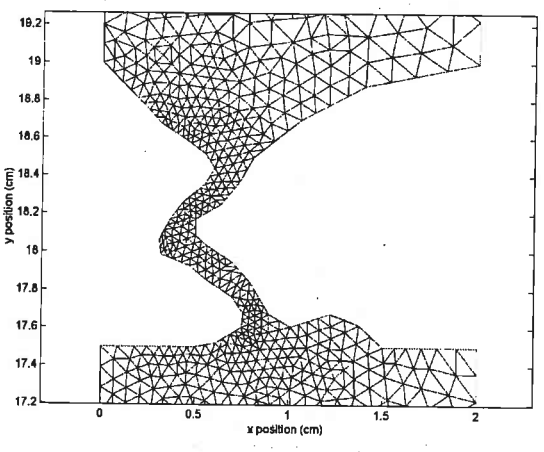

Figure 6: Mesh used for generating Figure 4.

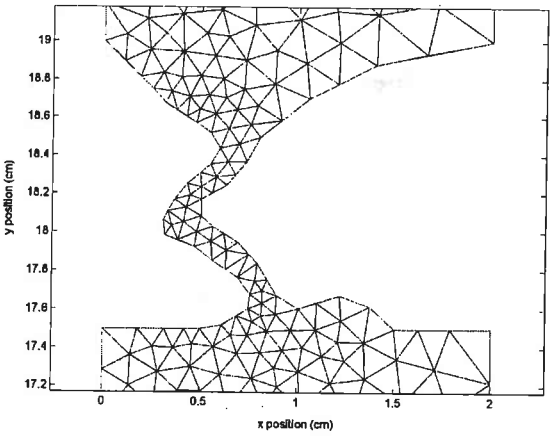

Figure 7: Mesh used for generating Figure 5.

4. DISCUSSION

Several issues affecting particle capture come to light from the investigation of the arbitrary geometry. Firstly, the initial position of the particles plays a part in where the particles will most likely be captured. For particles initially close to the walls of the cylinder, particle capture may occur at the bottom of the filter where the particles are unable to negotiate the bend into the pathway.

Because the filter considered is three dimensional, given an even initial distribution of particles across the cross-section, a greater proportion of particles will be closer to the edges of the cylinder than near the center. This suggests that even for a low velocity, a great proportion of particles will be captured by merit of proximity to the cylinder wall.

Secondly, for particles nearer to the center, the bend in the streamlines upon entering the pathway is minimal. Capture, if it occurs, is likely to be within the pathway due to its tortuousity and velocity. As it is expected that tortuousity of the pathway will decrease with increasing velocity, it is expected that the velocity-tortuousity trade-off will form some optimisation problem. The details of this require further investigation.

Thirdly, it is expected that higher velocities will increase the reliance upon a tortuous pathway for particle capture due to additional pathways. For higher velocities, it has been observed that additional pathways will form through the filter. The addition of pathways to the filter is expected to decrease the particle capture at the entrance to the filter, by reducing the area range of

streamlines entering each pathway. This will reduce the curvature of streamlines at the pathway edges entering a particular pathway. More particles will enter the pathway where they can only be captured within the pathway via tortuousity and velocity.

Fourth, the mesh used in the PDE Toolbox has a discernable effect upon the particle trajectory raising the question of how much of the capture observed in the experiments is due to the mesh. The fluid velocity used in the program for any point in space is the average of the velocity taken across the mesh cell. As the velocity near the air-water interface is taken as the average velocity of the mesh cell to which it belongs, the effect of defining the boundary condition to state that velocity normal to the boundary is zero may be negated. Capture of particles may occur due to this averaged velocity driving particles into the boundary rather than the particles drifting to the boundary due to inertia. Unfortunately, the computational time cost of refining the mesh more makes investigation of this effect difficult.

5. CONCLUSIONS

It has been shown that particles can be captured due to inertia in a bubbling filter. This capture relies upon a combination of factors including the particle's initial position, the air velocity and the tortuousity of the pathways. The effect of particle diameter has not been investigated in this paper.

Whether or not inertial capture is the primary mechanism behind the bubbling filter is yet to be answered. Although it has been demonstrated that inertial capture can occur, quantitative comparison with experiments is not possible with a two-dimensional model. The issue of the presence of bubbles and bubbling as a primary mechanism may be better answered by using NMR imaging to detect bubbles within the filter. The results of such experiments are not yet available.

Although factors have been identified that affect particle capture, interactions between these factors (most notably velocity and tortuousity) are yet to be investigated. These investigations also rely upon further NMR imaging.

The importance of the velocity and tortuousity of the pathway to capture suggests that further investigations seeking to improve these to factors, such as by varying filters used and choosing flow rates that simultaneously optimise these two factors, would prove the most fruitful towards the goal of improving filter efficiency.

The program used may be requested from NadiahKristensen@hotmail.com.

6. REFERENCES

Agranovski, I. E., R.D. Braddock, and T. Myojo, Removal of aerosols by bubbling through porous media, *Aerosol Science and Technology*, 31(4): 249, 1999a.

Agranovski, I. E., R.D. Braddock, S. Crozier, A. Whittaker, and S. Minty, Magnetic Resonance Imaging of gas flows in wet porous filters involved in aerosol removal processes, *Journal of Aerosol Science*, 30: 543, 1999b.

Agranovski, I. E., R.D. Braddock, and N. P. Kristensen, Model for the flow of air through a wet fibre, *Journal of Aerosol Science*, 31(Suppl 1): S688-S689, 2000a.

Agranovski, I. E., R.D. Braddock, N. P. Kristensen, S. Crozier, and T. Myojo, Study of the gas flow in porous media submerged in liquid layers, *Journal of Aerosol Science*, 31(Suppl 1): S454-S455, 2000b.

Bear, J. *Dynamics of Fluids in Porous Media,* Elsevier, New York, 162-164 pp., 1972

Evett, J. B., and C. Lin, *Fundamentals of Fluid Mechanics,* McGraw-Hill, London, 1987.

Fuchs, N., *The Mechanics of Aerosols*, Pergamon Press, Oxford, 240-245 pp., 1964.

Hinds, W. C., *Aerosol Technology: Properties, Behaviour, and Measurement of Airborne Particles,* John Wiley and Sons, 106-131 pp., 1982.

Prandtl, L. and O. G. Tietjens, *Applied Hydrodynamics and Aeromechanics,* Dover Publications, New York, 1934.